JOURNAL OF GUIDANCE, CONTROL, AND DYNAMICS
Vol. 17, No. 5, September–October 1994

Rendezvous Targeting and Navigation for a Translunar Halo Orbit

Brian L. Jones*
Air Force Institute of Technology, Wright-Patterson Air Force Base, Ohio 45433
and
Robert H. Bishop†
University of Texas at Austin, Austin, Texas 78712

Two-spacecraft terminal-phase rendezvous targeting and navigation are examined for the circular restricted three-body problem. A targeting law and navigation filter are developed assuming the traditional passive target-active chaser vehicle relationship. The targeting law is demonstrated using a small-radius translunar halo orbit and ideal navigation; the three-body terminal-phase rendezvous problem is then further characterized and contrasted with the two-body problem. Nonlinear simulation results validate the navigation filter design and provide data to assess the filter performance. To demonstrate the entire guidance and navigation system, two profiles for terminal-phase rendezvous were considered in a planar circular orbit and two equivalent profiles in an $\mathcal{H}_2$ guided halo orbit.

Introduction

FOR the past 25 years, halo orbits about three-body equilibrium points have been investigated. The initial applications considered were follow-on lunar exploration opportunities[1] and scientific data collection.[2] This second application was realized when, in 1978, the *International Sun-Earth Explorer-3* spacecraft was successfully placed into a halo orbit around the interior equilibrium point of the sun-Earth system.[3] More recently, the Space Exploration Initiative included a halo orbit in its mission scenarios.[4,5] Further, six more halo orbit applications have been proposed for the 1990s.[6] The research addresses an additional application by considering two-spacecraft terminal-phase rendezvous in a translunar halo orbit. It employs the traditional passive target–active chaser vehicle relationship in terminal-phase rendezvous. The target vehicle is in a small-radius halo orbit; its guidance law is restricted to controlling its own orbit. The chaser vehicle is in an independent small-radius halo orbit and executes all rendezvous maneuvers.

Many investigators have examined the halo orbit *guidance* problem (e.g., see Farquhar[7]). This paper will use the $\mathcal{H}_2$ optimal guidance presented in Jones and Bishop[8] for the target vehicle. By contrast, rendezvous *targeting* in the three-body problem is a relatively unexplored area. Successful two-spacecraft rendezvous were accomplished in the Gemini, Apollo, and Space Shuttle programs; however, the underlining system in all three cases was two-body motion. Relative *navigation* for rendezvous in the three-body problem is similarly unexplored. For the Earth-moon system, two significant publications[9,10] discuss the orbit determination of a single spacecraft about an equilibrium point. Additional publications[10,11] are found when considering other three-body systems.

This paper derives a terminal-phase rendezvous targeting law that is valid for the circular restricted three-body problem. Further, it will develop a rendezvous navigation filter capable of supplying accurate state information to this targeting law. The ultimate goal of this research is to characterize the three-body terminal-phase rendezvous problem.

Presented as Paper 93-144 at the AAS/AIAA Space Flight Mechanics Conference, Pasadena, CA, Feb. 22–24, 1993; received May 19, 1993; revision received Dec. 6, 1993; accepted for publication Dec. 20, 1993.

*Assistant Professor, Department of Aeronautics and Astronautics; Major, U.S. Air Force. Senior Member AIAA.

†Assistant Professor, Department of Aerospace Engineering and Engineering Mechanics. Senior Member AIAA.

Circular Restricted Problem of Three Bodies

The derivation of the nondimensional equations of motion for the circular restricted three-body problem is well known (e.g., see Szebehely[13]). The halo orbit guidance problem adds one additional term in each equation, U, corresponding to the control acceleration on the spacecraft. Hence,

$$\ddot{x} - 2\dot{y} - x = -\left(\frac{\mu[x-(1-\mu)]}{\rho_{MS}^3} + \frac{(1-\mu)[x+\mu]}{\rho_{ES}^3}\right) + U_x \tag{1}$$

$$\ddot{y} + 2\dot{x} - y = -y\left(\frac{\mu}{\rho_{MS}^3} + \frac{(1-\mu)}{\rho_{ES}^3}\right) + U_y \tag{2}$$

$$\ddot{z} = -z\left(\frac{\mu}{\rho_{MS}^3} + \frac{(1-\mu)}{\rho_{ES}^3}\right) + U_z \tag{3}$$

where

$$\rho_{MS} = \sqrt{[x-(1-\mu)]^2 + y^2 + z^2} \tag{4}$$

$$\rho_{ES} = \sqrt{[x+\mu]^2 + y^2 + z^2} \tag{5}$$

and (x, y, z) are the nondimensional position components of the spacecraft in each axis of the rotating coordinate system and μ is the mass ratio of the two primary bodies. Writing Eqs. (1–3) in functional matrix form yields

$$\dot{\boldsymbol{X}} = \boldsymbol{f}_1(\boldsymbol{X}(t)) + \boldsymbol{g}(\boldsymbol{U}(t)) \tag{6}$$

where

$$\boldsymbol{X} \triangleq \begin{bmatrix} x & y & z & \dot{x} & \dot{y} & \dot{z} \end{bmatrix}^T, \qquad \boldsymbol{U} \triangleq \begin{bmatrix} U_x & U_y & U_z \end{bmatrix}^T \tag{7}$$

Define the linearized state and control as

$$\boldsymbol{\Omega} \triangleq \boldsymbol{X} - \boldsymbol{X}_{\text{nom}}, \qquad \boldsymbol{u} \triangleq \boldsymbol{U} - \boldsymbol{U}_{\text{nom}} \tag{8}$$

where $(\cdot)_{\text{nom}}$ denotes a nominal value. Neglecting the higher order terms in a Taylor series expansion yields

$$\dot{\boldsymbol{\Omega}} = \boldsymbol{A}_G\boldsymbol{\Omega} + \boldsymbol{B}_G\boldsymbol{u} \tag{9}$$

where

$$\boldsymbol{A}_G = \left[\frac{\partial \boldsymbol{f}_1}{\partial \boldsymbol{X}}\right]_{\text{nom}}, \qquad \boldsymbol{B}_G = \left[\frac{\partial \boldsymbol{g}}{\partial \boldsymbol{U}}\right]_{\text{nom}} \tag{10}$$

The nominal value for the translunar equilibrium point is

$$x = 1.155682, \qquad y = z = \dot{x} = \dot{y} = \dot{z} = 0 \tag{11}$$

which results in

$$\boldsymbol{A}_G = \begin{bmatrix} \boldsymbol{0} & \boldsymbol{I} \\ \boldsymbol{A}_{G21} & \boldsymbol{A}_{G22} \end{bmatrix}, \qquad \boldsymbol{B}_G = \begin{bmatrix} \boldsymbol{0} \\ \boldsymbol{I} \end{bmatrix} \tag{12}$$

where

$$\boldsymbol{A}_{G21} = \begin{bmatrix} 7.380861 & 0 & 0 \\ 0 & -2.190431 & 0 \\ 0 & 0 & -3.190431 \end{bmatrix} \tag{13}$$

$$\boldsymbol{A}_{G22} = \begin{bmatrix} 0 & 2 & 0 \\ -2 & 0 & 0 \\ 0 & 0 & 0 \end{bmatrix} \tag{14}$$

Rendezvous Targeting Law

Consider the terminal-phase rendezvous of two spacecraft about the translunar equilibrium point. Assume the target vehicle is in a small-radius halo orbit and is controlling its own orbit using an unknown guidance law. The target vehicle orbits described by Jones and Bishop[8] can be approximated by an ellipse inclined to the y-z plane. The equations of motion for this approximation are

$$\boldsymbol{\Psi}_{\text{tp}} = \begin{bmatrix} x_{t_{\max}} \sin(ft + \psi_x) \\ y_{t_{\max}} \sin(ft + \psi_y) \\ z_{t_{\max}} \sin(ft + \psi_z) \end{bmatrix} \qquad \text{and} \qquad \boldsymbol{\Psi}_{\text{tv}} = \dot{\boldsymbol{\Psi}}_{\text{tp}} \tag{15}$$

which leads to the state equation

$$\begin{bmatrix} \dot{\boldsymbol{\Psi}}_{\text{tp}} \\ \dot{\boldsymbol{\Psi}}_{\text{tv}} \end{bmatrix} = \boldsymbol{A}_p \begin{bmatrix} \boldsymbol{\Psi}_{\text{tp}} \\ \boldsymbol{\Psi}_{\text{tv}} \end{bmatrix} \tag{16}$$

where

$$\boldsymbol{A}_p = \begin{bmatrix} \boldsymbol{0} & \boldsymbol{I} \\ -f^2\boldsymbol{I} & \boldsymbol{0} \end{bmatrix} \tag{17}$$

and f is the halo orbit frequency. The subscripts tp and tv denote the target vehicle's position and velocity, respectively.

Because the halo orbits being considered have a small radius, the linearized equations of motion are valid for the chaser vehicle. Further, during a rendezvous profile the chaser vehicle will terminate its own halo orbit guidance. Hence, the chaser vehicle's state equation becomes

$$\begin{bmatrix} \dot{\boldsymbol{\Omega}}_{\text{cp}} \\ \dot{\boldsymbol{\Omega}}_{\text{cv}} \end{bmatrix} = \boldsymbol{A}_G \begin{bmatrix} \boldsymbol{\Omega}_{\text{cp}} \\ \boldsymbol{\Omega}_{\text{cv}} \end{bmatrix} \tag{18}$$

where $\boldsymbol{A}_G$ is defined by Eq. (12) and the subscripts cp and cv denote the chaser vehicle's position and velocity, respectively.

Defining the relative position and velocity as

$$\begin{bmatrix} \boldsymbol{\delta}_p \\ \boldsymbol{\delta}_v \end{bmatrix} \triangleq \begin{bmatrix} \boldsymbol{\Omega}_{\text{cp}} - \boldsymbol{\Psi}_{\text{tp}} \\ \boldsymbol{\Omega}_{\text{cv}} - \boldsymbol{\Psi}_{\text{tv}} \end{bmatrix} \tag{19}$$

leads to an augmented state equation for the relative and target vehicle states, which can be solved analytically in terms of a 4×4 block state transition matrix. The state transition matrix $\boldsymbol{\Phi}$ is a function of exponentially increasing and decreasing terms as well as sinusoidal terms at three different natural frequencies; $\boldsymbol{\Phi}$ is further detailed in the Appendix.

The necessary and sufficient conditions for rendezvous are that the relative position and velocity at the time of rendezvous be a specified value. Consider a two-maneuver terminal-phase rendezvous sequence where the first maneuver is executed at the beginning of the rendezvous (t_1) and designed so that the chaser vehicle will coast to the specified relative position at the time of rendezvous (t_2); the second maneuver is then executed to satisfy the specified relative velocity condition.

The terminal-phase initiation maneuver (TI) is defined as

$$\Delta \boldsymbol{V}_{\text{TI}} \triangleq \boldsymbol{\Omega}_{\text{cv}}(t_1^+) - \boldsymbol{\Omega}_{\text{cv}}(t_1^-) = \boldsymbol{\delta}_v(t_1^+) - \boldsymbol{\delta}_v(t_1^-) \tag{20}$$

where the minus and plus superscripts denote immediately before and immediately after a specified time, respectively. Given $\boldsymbol{\Phi}$, Eq. (20) can be expressed in terms of the specified position at the end of the rendezvous, the initial relative position and velocity, and the chaser vehicle's initial position and velocity:

$$\Delta \boldsymbol{V}_{\text{TI}} = \boldsymbol{\phi}_{12}^{-1}\big[\boldsymbol{\delta}_p(t_2^+) + (\boldsymbol{\phi}_{13} - \boldsymbol{\phi}_{11})\boldsymbol{\delta}_p(t_1^-) + (\boldsymbol{\phi}_{14} - \boldsymbol{\phi}_{12})\boldsymbol{\delta}_v(t_1^-) - \boldsymbol{\phi}_{13}\boldsymbol{\Omega}_{\text{cp}}(t_1^-) - \boldsymbol{\phi}_{14}\boldsymbol{\Omega}_{\text{cv}}(t_1^-)\big] \tag{21}$$

Note that this targeting law requires only relative state information, which can be provided by an onboard navigation filter using a proximity sensor and chaser vehicle state information. Hence, no target vehicle specific information is required. Additionally, Eq. (21) contains a numerical singularity at specific transfer times. That is, when

$$\Delta t = t_2 - t_1 = \frac{k\pi}{1.786178} \sim k \times 7.637724 \text{ days}, \qquad k = 1, 2, \ldots \tag{22}$$

the ϕ_{129} element becomes zero, causing the $\boldsymbol{\phi}_{12}$ submatrix to become singular. The ϕ_{129} element corresponds to the uncoupled z axis in the linearized equations of motion. These singularities do not limit this research because the transfer times considered here are much shorter than any singularity time.

Lastly, the terminal-phase final maneuver (TF) is defined as

$$\Delta \boldsymbol{V}_{\text{TF}} \triangleq \boldsymbol{\Omega}_{\text{cv}}(t_2^+) - \boldsymbol{\Omega}_{\text{cv}}(t_2^-) = \boldsymbol{\delta}_v(t_2^+) - \boldsymbol{\delta}_v(t_2^-) \tag{23}$$

Rendezvous Navigation Filter

The rendezvous navigation filter is formulated assuming the estimated states are the chaser vehicle's inertial state, unmodeled accelerations on the chaser vehicle, and measurement biases. It is assumed that either the target vehicle or its mission control center will supply the chaser vehicle with target vehicle state information at the time of each measurement. Muller and Kachmar[14] showed the equivalence of optimally estimating the relative state or optimally estimating the inertial state of one spacecraft and subtracting it from an externally supplied inertial state of the other spacecraft. This estimation is optimal in the sense that it yields the minimum relative state error at the time of measurement incorporation, not necessarily the minimum relative state error over the entire navigation period. The navigation filter is implemented in the nonlinear simulation such that the chaser vehicle's inertial state is always estimated and the other estimation states are selectable.

The dynamical system for the chaser vehicle can be described by a continuous nonlinear differential equation

$$\dot{\boldsymbol{X}}_c(t) = \boldsymbol{f}_1(\boldsymbol{X}_c(t)) + \boldsymbol{a}(t) \tag{24}$$

where $\boldsymbol{f}_1(\boldsymbol{X}_c(t))$ is given by Eq. (6) and $\boldsymbol{a}(t)$ represents unmodeled accelerations. Assume the unmodeled accelerations have the form of a first-order Gauss-Markov process,

$$\dot{\boldsymbol{a}}(t) = \boldsymbol{A}_a\boldsymbol{a}(t) + \boldsymbol{w}_a(t) \tag{25}$$

where $\boldsymbol{A}_a$ is a diagonal dynamics matrix and $\boldsymbol{w}_a(t)$ is white Gaussian noise with zero mean and $\boldsymbol{Q}_a$ fixed power spectrum. The discrete nonlinear measurements are modeled as

$$\boldsymbol{y}(t_k) = \boldsymbol{h}_1(\boldsymbol{X}_c(t_k)) + \boldsymbol{b}(t_k) + \boldsymbol{v}(t_k); \qquad k = 1, 2, \ldots \tag{26}$$

where $\boldsymbol{h}_1(\boldsymbol{X}_c(t_k))$ represents the measurement-state relationships. The measurement bias $\boldsymbol{b}(t_k)$ is also modeled as a first-order Gauss-Markov process

$$\dot{\boldsymbol{b}}(t) = \boldsymbol{A}_b\boldsymbol{b}(t) + \boldsymbol{w}_b(t) \tag{27}$$

where $\boldsymbol{A}_b$ is a diagonal dynamics matrix and $\boldsymbol{w}_b(t)$ is white Gaussian noise with zero mean and $\boldsymbol{Q}_b$ fixed power spectrum. The measurement noise $\boldsymbol{v}(t_k)$ is also white Gaussian noise with zero mean and $\boldsymbol{R}_k$ covariance matrix.

Define an estimation state vector

$$\mathbf{Z}(t) \triangleq \begin{bmatrix} \mathbf{X}_c^T(t) & \mathbf{a}^T(t) & \mathbf{b}^T(t) \end{bmatrix}^T \tag{28}$$

Combining Eqs. (24), (25), and (27) yields

$$\dot{\mathbf{Z}}(t) = \mathbf{f}_2(\mathbf{Z}(t)) + \mathbf{w}(t) \tag{29}$$

where

$$\mathbf{w}(t) \triangleq \begin{bmatrix} \mathbf{0} & \mathbf{w}_a^T(t) & \mathbf{w}_b^T(t) \end{bmatrix}^T \tag{30}$$

and is white Gaussian noise with zero mean and $\mathbf{Q}$ fixed power spectrum.

Finally, Eq. (26) can be rewritten as

$$\mathbf{y}(t_k) = \mathbf{h}_2(\mathbf{Z}(t_k)) + \mathbf{v}(t_k) \tag{31}$$

Equations (29) and (31) give the standard form of the dynamical system for the continuous-discrete Kalman filter. The derivation of the propagation and update equations for this filter is well known (e.g., see Gelb[15]). The estimation state propagation equation is

$$\dot{\hat{\mathbf{Z}}}(t) = E[\mathbf{f}_2(\mathbf{Z}(t))] \approx \mathbf{f}_2(\hat{\mathbf{Z}}(t)); \qquad t_k \le t \le t_{k+1} \tag{32}$$

where sensor measurements are available at t_k and t_{k+1}. Propagation of the error covariance matrix is accomplished via

$$\dot{\mathbf{P}}(t) = \mathbf{P}(t)\mathbf{F}^T(t) + \mathbf{F}(t)\mathbf{P}(t) + \mathbf{Q} \tag{33}$$

where

$$\mathbf{F}(t) \triangleq \left.\frac{\partial \mathbf{f}_2(\mathbf{Z}(t))}{\partial \mathbf{Z}(t)}\right|_{\mathbf{Z}(t)=\hat{\mathbf{Z}}(t)} \tag{34}$$

The estimation state and error covariance matrix are updated according to

$$\hat{\mathbf{Z}}(t_k^+) = \hat{\mathbf{Z}}(t_k^-) + \mathbf{K}(t_k)[\mathbf{y}(t_k) - \mathbf{h}_2(\hat{\mathbf{Z}}(t_k^-))] \tag{35}$$

$$\mathbf{P}(t_k^+) = [\mathbf{I} - \mathbf{K}(t_k)\mathbf{H}(t_k)]\mathbf{P}(t_k^-)[\mathbf{I} - \mathbf{K}(t_k)\mathbf{H}(t_k)]^T + \mathbf{K}(t_k)\mathbf{R}_k\mathbf{K}^T(t_k) \tag{36}$$

where the minus and plus superscripts denote immediately before and immediately after measurement incorporation, respectively, and

$$\mathbf{K}(t_k) \triangleq \mathbf{P}(t_k^-)\mathbf{H}^T(t_k)\left[\mathbf{H}(t_k)\mathbf{P}(t_k^-)\mathbf{H}^T(t_k) + \mathbf{R}_k\right]^{-1} \tag{37}$$

$$\mathbf{H}(t_k) \triangleq \left.\frac{\partial \mathbf{h}_2(\mathbf{Z}(t_k))}{\partial \mathbf{Z}(t_k)}\right|_{\mathbf{Z}(t_k)=\hat{\mathbf{Z}}(t_k^-)} \tag{38}$$

For this research, the set of measurements consists of

$$\mathbf{h}_1(\mathbf{X}_c(t_k)) = \begin{bmatrix} R & \dot{R} & \phi & \theta \end{bmatrix}^T \tag{39}$$

where R is the relative range between the chaser and target vehicles, $\dot{R}$ is the relative range rate, and ϕ and θ are the roll and pitch angles of the relative position vector in the chaser vehicle's body coordinates. The detailed derivative of the measurement-state relationships is contained in Jones.[16]

Simulation Results

A nonlinear simulation was developed to model the three-body terminal-phase rendezvous problem. The simulation computes TI, TF, and up to eight midcourse correction (MCC) maneuvers using Eqs. (21) and (23). For analysis purposes, an option was implemented that will place the target vehicle in a planar circular orbit inclined to the y-z plane rather than in an actual $\mathcal{H}_2$ guided halo orbit. A positive incline angle is defined as a positive rotation about the y axis. This option eliminates the target vehicle trajectory approximation used in the development of Eq. (21). In addition, an initial condition angle was defined to indicate the position on the halo orbit of the TI maneuver; the initial-condition angle is measured from the bottom of the halo orbit in a clockwise direction. For all profiles, clockwise orbits were used, the chaser vehicle initiated the rendezvous profile approximately 19 km behind the target vehicle, and the position and velocity offset at rendezvous was specified to be zero.

To investigate the three-body rendezvous characteristics, ideal navigation was initially assumed. The first characteristic investigated was final position error at the time of rendezvous due to the TI targeting law. Figure 1 shows constant error contours as a function of transfer time and initial condition angle. The maximum final position error occurs when TI occurs at the left or right sides of the halo orbit. These points correspond to the points of maximum curvature of the actual halo orbit resulting in the largest difference between the target vehicle's orbit approximation and the actual halo orbit. Further, the final position error was generally in the out-of-plane direction.

The second three-body rendezvous characteristic investigated was the effect of transfer time and initial condition angle on the geometry of the rendezvous profile. A planar circular orbit was used to ensure final position errors were less than 1 m. The incline angle was fixed at 22.85 deg, which corresponded to the incline angle of the actual halo orbit used in this research. Figure 2 shows the minimum out-of-plane relative position (dashed lines) achieved by the rendezvous profile as a function of the input parameters. Also shown in Fig. 2 are lines of total propulsive cost of the rendezvous profile (solid lines). Two characteristics were observed. First, for every initial condition angle there is a transfer time that produces a minimum total propulsive cost of the rendezvous profile (e.g., 180 deg, 13 h). Second, total propulsive costs increase with out-of-plane relative motion.

The third three-body rendezvous characteristic investigated was the effect of incline angle and initial condition angle on the geometry of the rendezvous profile. As before, a planar circular orbit was used to ensure final position errors were less than 1 m. The transfer time was fixed at the baseline case value of 9 h. Figure 3 shows the same general information as Fig. 2 except incline angle has replaced transfer time. These results show that a minimum total propulsive cost rendezvous profile is a function of incline angle as well as initial condition angle and transfer time.

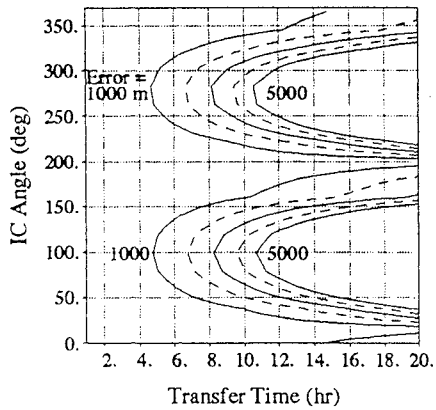

Fig. 1 *TI* **targeting law error.**

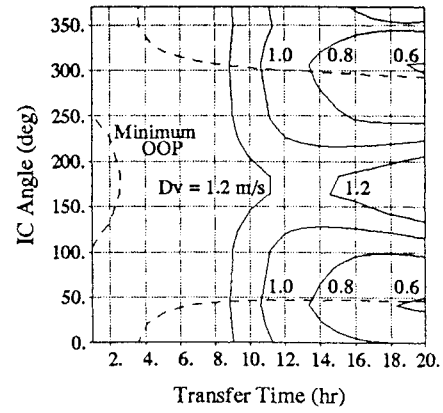

Fig. 2 Constant incline angle characteristics.

Table 1 Propulsion requirements summary

Error vector	Rendezvous maneuver, m/s							RCS fuel, lbs
	TI	MCC1	MCC2	MCC3	MCC4	TF	Total	
Circle 1								
Reference	0.686	0.000	0.000	0.000	0.000	0.491	1.177	5.776
Average	0.686	0.041	0.010	0.010	0.014	0.493	1.254	6.153
Circle 2								
Reference	0.680	0.000	0.000	0.000	0.000	0.643	1.322	6.487
Average	0.680	0.041	0.009	0.008	0.014	0.634	1.384	6.791
Halo 1								
Reference	0.627	0.019	0.022	0.027	0.044	0.684	1.421	6.972
Average	0.627	0.041	0.023	0.032	0.042	0.677	1.441	7.071
Halo 2								
Reference	0.704	0.008	0.008	0.009	0.013	0.672	1.413	6.933
Average	0.704	0.042	0.013	0.012	0.021	0.663	1.455	7.139

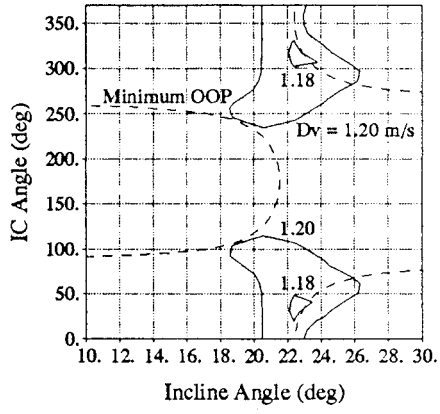

Fig. 3 Constant transfer time characteristics.

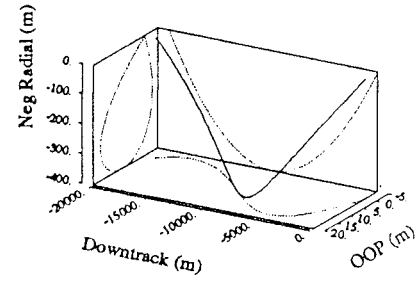

IC = 46.08 deg, Incline = 22.85 deg

Fig. 4 In-plane rendezvous profile.

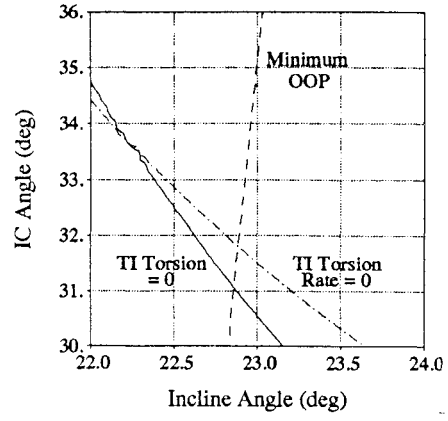

Fig. 5 Relative trajectory torsion and rate of change of torsion at terminal-phase rendezvous initiation.

Finally, Fig. 4 summarizes the geometry of the "in-plane" rendezvous profile. For a fixed incline angle and increasing initial condition angle in the vicinity of the "in-plane" profile, the out-of-plane component switches from away from the moon (positive x) to toward the moon (negative x). This same characteristic is observed for a fixed initial condition angle and decreasing incline angle in the vicinity of the "in-plane" profile. Figure 4 also shows that the relative trajectory is three dimensional. A necessary condition for the relative trajectory to be two dimensional is that the torsion and rate of change of torsion be zero at the initiation of the rendezvous profile. Figure 5 shows contours of zero torsion and zero rate of change of torsion at TI; also shown is the minimum out-of-plane contour from Fig. 3. For the relative trajectory to be two dimensional and lie in the target vehicle's halo orbit plane, the three contours must intersect at the same point. Hence, two dimensional relative trajectories do not exist. However, the minimum out-of-plane contour from Fig. 3 represents a maximum out-of-plane distance on the order of 10 m. Thus, these relative trajectories are essentially "in-plane" and are referred to as such in this paper. Additional detail on the targeting law characteristics can be found in Jones and Bishop.[17]

The rendezvous navigation filter was initialized with an error vector added to the chaser vehicle to model the uncertainty in the state just prior to the TI maneuver. Error vectors were generated randomly using error statistics consistent with Gingiss[9]; each one corresponded to a constant 1σ error from the six-dimensional error ellipsoid at the TI maneuver. Potter[18] and Hitzl[19] both describe the technique used in choosing these vectors. Additionally, these vectors were chosen to span all directions of the TI error ellipsoid.

Sensor measurements consisted of relative range and line-of-sight angles and were taken every minute. Measurement statistics and sensor capabilities were chosen similar to the Space Shuttle rendezvous radar[20] and were consistent with an advanced rendezvous tracking system study.[21] Random noise was added to each measurement, but measurement biases and unmodeled accelerations were omitted from the estimation vector. State estimation errors converged quickly after only a few measurements were incorporated.

The optimal placement of a midcourse correction maneuver within the rendezvous profile depends on the navigation errors at the time of the maneuver and the sensitivity of the final position errors at the time of rendezvous with respect to maneuver velocity errors. Figure 6a shows the time history of the magnitude of the principal axes of the local vertical inertial rectangular (LVIR) covariance velocity error ellipsoid along the baseline "in-plane" rendezvous profile; Fig. 6b gives the LVIR orientation of the largest principal axis of the covariance velocity error ellipsoid. Note that, even though the error ellipsoid loses its spherical shape, it shrinks at an essentially uniform rate and the absolute magnitude of all of the principal axes is small after only a few measurements have been incorporated into the filter. In addition, the sensitivity of the final-position errors with respect to maneuver velocity errors was computed. The maximum singular value of the sensitivity matrix showed a linear relationship along the baseline "in-plane" rendezvous profile. Thus, the placement of a midcourse correction maneuver is not strongly influenced by navigation errors or final position error sensitivities. Hence, the midcourse correction maneuvers can be placed in the rendezvous profile based on time.

To demonstrate the entire guidance and navigation system, two profiles were considered for terminal-phase rendezvous in the pla-

Table 2 Final miss distance summary

	Final miss distance, m			
	Downtrack	Out-of-plane	Radial	Total
Circle 1				
Reference	0.000	−0.001	0.000	0.001
Average magnitude	4.919	7.204	6.983	12.666
Circle 2				
Reference	0.000	0.000	−0.001	0.001
Average magnitude	8.086	9.779	5.686	15.362
Halo 1				
Reference	−7.673	19.394	0.124	20.857
Average magnitude	9.160	19.585	9.303	25.924
Halo 2				
Reference	−4.834	−3.191	−0.885	5.859
Average magnitude	5.898	10.222	5.036	14.109

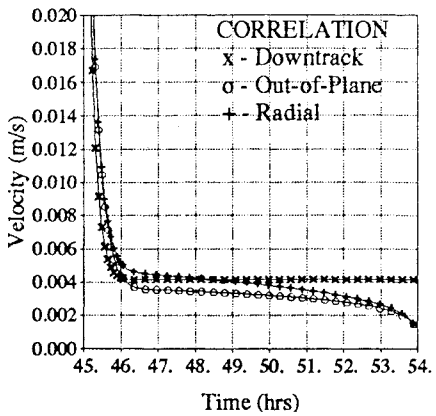

a) Magnitude of convariance principle axes

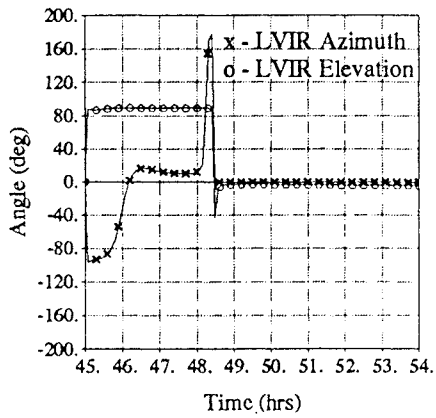

b) Angle to largest principle axis

Fig. 6 Covariance velocity error ellipsoid.

nar circular orbit and two equivalent profiles in an $\mathcal{H}_2$ guided halo orbit. The two profiles chosen correspond to "in-plane" (profile 1) and "out-of-plane" (profile 2) relative trajectories for the planar circular orbit. These same initial conditions were used in an $\mathcal{H}_2$ guided halo orbit demonstration. Monte Carlo simulations were completed and, for comparison purposes, a reference simulation was also done assuming "ideal" navigation. Four evenly spaced midcourse correction maneuvers were added to the rendezvous profile to correct for rendezvous targeting and rendezvous navigation filter state estimation errors.

Table 1 summarizes the propulsion requirements for both the planar circular orbit and the $\mathcal{H}_2$ guided halo orbit. The initial spacecraft weight was assumed to be the maximum allowed (13,000 lb) under the assumptions of the restricted three-body problem. Also, a medium-performance reaction control system (RCS) jet ($I_{sp} = 270$ s) was assumed. Table 2 shows the final miss distance for both demonstrations. Rendezvous profile changes from "in-plane" to "out-of-plane" resulted in increases in velocity requirements and

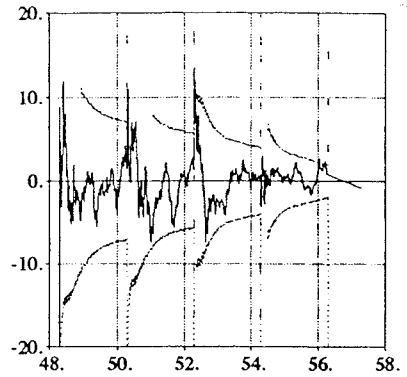

a) Max pos error (m) vs time (hrs)

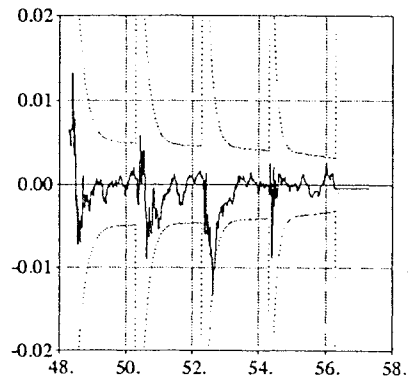

b) Max vel error (m/s) vs time (hrs)

Fig. 7 Maximum chaser vehicle state estimation error.

final miss distances. This same result was also seen for the addition of state estimation errors. When considering the absolute magnitude of these changes, the planar circular orbit displayed essentially the same characteristics as the $\mathcal{H}_2$ guided halo orbit. Even though these increases due to relative trajectory differences and rendezvous navigation filter state estimation errors could be considered significant, it should be noted that the absolute propulsion requirements and final miss distance were small in each profile.

State estimation errors from the rendezvous navigation filter were small in each profile. Figure 7 shows the maximum of the average position and velocity state estimation errors of the four profiles (solid line) and the associated 1σ standard deviation of the state (dotted line). The rendezvous navigation filter performance was not substantially affected by the geometry of the four relative trajectories. Additional detail on the rendezvous navigation filter characteristics can be found in Jones and Bishop.[22]

Conclusions

A two-spacecraft terminal-phase rendezvous targeting law has been developed that is valid for the circular restricted three-body problem. This targeting law was demonstrated using a small-radius translunar halo orbit and ideal navigation. Several characteristics of three-body rendezvous were observed. First, terminal-phase rendezvous in the circular restricted three-body problem is three dimensional; out-of-plane relative motion with respect to the target vehicle occurs. Second a design trade-off exists between targeting law error, out-of-plane relative motion, and the total propulsive cost of the rendezvous profile. Third, final out-of-plane errors generally dominate both downtrack and radial errors. Lastly, a minimum total propulsive cost rendezvous profile exists and is a function of transfer time, incline angle, and initial condition angle. A rendezvous navigation filter capable of supplying the rendezvous targeting law with chaser vehicle state information was then developed. Estimation errors converged quickly after only a few relative range and line-of-sight angle measurements were incorporated. The placement of a midcourse correction maneuver was not directly dependent on navigation errors or final position error sensitivities. Four total cases, two rendezvous profiles for the translunar planar circular orbit and

two equivalent rendezvous profiles for the $\mathcal{H}_2$ guided translunar halo orbit, were examined to demonstrate the entire guidance and navigation system. In each case, total propulsion requirements were less than 1.5 m/s and final miss distance was less than 26 m. State estimation errors were small and showed no substantial performance degradation due to the rendezvous profile geometry. The translunar planar circular orbit displayed the same characteristics as the $\mathcal{H}_2$ guided translunar halo orbit, although the propulsion requirements and final miss distance were generally larger in the $\mathcal{H}_2$ guided demonstration.

Appendix

The rendezvous targeting law given in Eq. (21) is dependent on the 4×4 block state transition matrix computed from the augmented state equation for the relative and target vehicle states. Each block of interest in the state transition matrix has the form

$$\phi_{1k} = \begin{bmatrix} \phi_{1k1} & \phi_{1k2} & 0 \\ \phi_{1k4} & \phi_{1k5} & 0 \\ 0 & 0 & \phi_{1k9} \end{bmatrix}, \qquad k = 1, 2, 3, 4 \tag{A1}$$

Further, the ϕ_{13} and ϕ_{14} blocks are related to the ϕ_{11} and ϕ_{12} blocks by

$$\phi_{13} = \phi_{11} - \cos(f\Delta t)\boldsymbol{I} \tag{A2}$$

$$\phi_{14} = \phi_{12} - \frac{1}{f}\sin(f\Delta t)\boldsymbol{I} \tag{A3}$$

Solving for the specific elements of interest yields

$$\phi_{111} = c_1 e^{\tau\Delta t} + c_1 e^{-\tau\Delta t} - c_2 \cos(\omega_1 \Delta t) \tag{A4}$$

$$\phi_{112} = -c_3 e^{\tau\Delta t} + c_3 e^{-\tau\Delta t} + c_4 \sin(\omega_1 \Delta t) \tag{A5}$$

$$\phi_{114} = -c_5 e^{\tau\Delta t} + c_5 e^{-\tau\Delta t} + c_6 \sin(\omega_1 \Delta t) \tag{A6}$$

$$\phi_{115} = c_7 e^{\tau\Delta t} + c_7 e^{-\tau\Delta t} + c_8 \cos(\omega_1 \Delta t) \tag{A7}$$

$$\phi_{119} = \cos(\omega_2 \Delta t) \tag{A8}$$

$$\phi_{121} = c_9 e^{\tau\Delta t} - c_9 e^{-\tau\Delta t} + c_{10} \sin(\omega_1 \Delta t) \tag{A9}$$

$$\phi_{122} = c_{11} e^{\tau\Delta t} + c_{11} e^{-\tau\Delta t} - c_{12} \cos(\omega_1 \Delta t) \tag{A10}$$

$$\phi_{124} = -\phi_{122} \tag{A11}$$

$$\phi_{125} = -c_{13} e^{\tau\Delta t} + c_{13} e^{-\tau\Delta t} + c_{14} \sin(\omega_1 \Delta t) \tag{A12}$$

$$\phi_{129} = c_{15} \sin(\omega_2 \Delta t) \tag{A13}$$

where

$$\begin{aligned} \tau &= 2.158677, & \omega_1 &= 1.862647, & \omega_2 &= 1.786178 \\ c_1 &= 0.667355, & c_2 &= 0.334710, & c_3 &= 0.124821 \\ c_4 &= 0.289317, & c_5 &= 0.420595, & c_6 &= 0.974880 \\ c_7 &= 0.078667, & c_8 &= 0.842666, & c_9 &= 0.195181 \\ c_{10} &= 0.084468, & c_{11} &= 0.123011, & c_{12} &= 0.246022 \\ c_{13} &= 0.077527, & c_{14} &= 0.716566, & c_{15} &= 0.559855 \end{aligned}$$

and Δt is the rendezvous profile transfer time with f denoting the halo orbit frequency.

References

[1]Farquhar, R. W., "Future Missions for Libration-Point Satellites," *Astronautics and Aeronautics*, Vol. 7, No. 5, 1969, pp. 52–56.

[2]Farquhar, R. W., Muhonen, D. P., and Richardson, D. L., "Mission Design for a Halo Orbiter of the Earth," *Journal of Spacecraft and Rockets*, Vol. 14, No. 3, 1977, pp. 170–177.

[3]Farquhar, R. W., Muhonen, D. P., Newman, C. R., and Heuberger, H. S., "Trajectories and Orbital Maneuvers for the First Libration-Point Satellite," *Journal of Guidance, Control, and Dynamics*, Vol. 3, No. 6, 1980, pp. 549–554.

[4]"America at the Threshold: Report of the Synthesis Group on America's Space Exploration Initiative," U.S. Government Printing Office, Washington, DC, May 1991.

[5]"Report of the 90-Day Study on Human Exploration of the Moon and Mars," NASA, Washington DC, Nov. 1989.

[6]Farquhar, R. W., "Halo-Orbit and Lunar-Swingby Missions of the 1990's," *Acta Astronautica*, Vol. 24, 1991, pp. 227–234.

[7]Farquhar, R. W., "The Control and Use of Libration-Point Satellites," NASA-TR-R-346, Sept. 1970.

[8]Jones, B. L., and Bishop, R. H., "$\mathcal{H}_2$ Optimal Halo Orbit Guidance," *Journal of Guidance, Control, and Dynamics*, Vol. 16, No. 6, 1993, pp. 1118–1124.

[9]Gingiss, A. J., "Navigation Analysis of Earth-Moon Libration Point Missions," M.S. Thesis, Massachusetts Inst. of Technology, The Charles Stark Draper Laboratory Rep. CSDL-T-1133, Cambridge, MA, June 1992.

[10]Porter, J. D., "Final Report for Lunar Libration Point Flight Dynamics Study," NASA-CR-130135, Washington, DC, April 1969.

[11]Gordon, S. C., and Howell, K. C., "Orbit Determination Error Analysis and Comparison of Station-Keeping Costs for Lissajous and Halo-Type Libration Point Orbits," *Advances in Astronautical Sciences*, Vol. 79, Part I, 1992, pp. 117–136.

[12]Efron, L., Yeomans, D. K., and Schanzle, A. F., "ISEE-3/ICE Navigation Analysis," *Journal of Astronautical Sciences*, Vol. 33, No. 3, 1985, pp. 301–323.

[13]Szebehely, V., *Theory of Orbits: The Restricted Problem of Three Bodies*, Academic Press, New York, 1967.

[14]Muller, E. S., Jr., and Kachmar, P. M., "The Apollo Rendezvous Navigation Filter Theory, Description and Performance," The Charles Stark Draper Laboratory, Rept.-649, Cambridge, MA, June 1970.

[15]Gelb, A. (ed.), *Applied Optimal Estimation*, MIT Press, Cambridge, MA, 1974.

[16]Jones, B. L., "A Guidance and Navigation System for Two Spacecraft Rendezvous in Translunar Halo Orbit," Ph.D. Dissertation, Univ. of Texas at Austin, Austin, TX, May 1993.

[17]Jones, B. L., and Bishop, R. H., "Stable Orbit Rendezvous for a Small Radius Translunar Halo Orbit," *Advances in Astronautical Sciences*, Vol. 82, Part I, 1993, pp. 585–604.

[18]Potter, J. E., "Error Ellipsoids," Massachusetts Inst. of Technology Instrumentation Laboratory, Space Guidance Analysis Memo 29, Cambridge, MA, Nov. 1962.

[19]Hitzl, D. L., "A Note on Equiprobability Ellipsoids," *Journal of Astronautical Sciences*, Vol. 40, No. 1, 1992, pp. 165–170.

[20]"Onboard Navigation System Characteristics," NASA-JSC-14675, Rev. 1, Houston, TX, Dec. 1981.

[21]Laurie, R. J., and Sterzer, F., "Advanced Multipurpose Rendezvous Tracking System Study," NASA-CR-167708, Washington, DC, June 1982.

[22]Jones, B. L., and Bishop, R. H., "Rendezvous Navigation for a Two Spacecraft Stable Orbit Rendezvous in a Small Radius Translunar Halo Orbit," *Proceedings of the 1993 AIAA Guidance, Navigation, and Control Conference*, AIAA, Washington, DC, 1993, pp. 1403–1411.